Nuclear Engineering and Technology 53 (2021) 2960–2967

Contents lists available at ScienceDirect

Nuclear Engineering and Technology

journal homepage: www.elsevier.com/locate/net

Original Article

A hardening model considering grain size effect for ion-irradiated polycrystals under nanoindentation

Kai Liu [a], Xiangyun Long [a], Bochuan Li [a], Xiazi Xiao [b, **], Chao Jiang [a, *]

[a] State Key Laboratory of Advanced Design and Manufacturing for Vehicle Body, College of Mechanical and Vehicle Engineering, Hunan University, 410082 Changsha, China
[b] Department of Mechanics, School of Civil Engineering, Central South University, Changsha, 410075, PR China

ARTICLE INFO

Article history:
Received 18 August 2020
Received in revised form
30 January 2021
Accepted 7 March 2021
Available online 15 March 2021

Keywords:
Hardness
Ion irradiation
Grain size effect
Theoretical model
Nanoindentation

ABSTRACT

In this work, a new hardening model is proposed for the depth-dependent hardness of ion-irradiated polycrystals with obvious grain size effect. Dominant hardening mechanisms are addressed in the model, including the contribution of dislocations, irradiation-induced defects and grain boundaries. Two versions of the hardening model are compared, including the linear and square superposition models. A succinct parameter calibration method is modified to parametrize the models based on experimentally obtained hardness vs. indentation depth curves. It is noticed that both models can well characterize the experimental data of unirradiated polycrystals; whereas, the square superposition model performs better for ion-irradiated materials, therefore, the square superposition model is recommended. In addition, the new model separates the grain size effect from the dislocation hardening contribution, which makes the physical meaning of fitted parameters more rational when compared with existing hardness analysis models.

1. Introduction

Radiation damage is one of the main safety threats in nuclear industry. Studying the mechanical behavior of materials under radiation conditions is vital not only for the safe and reliable operation of nuclear reactors, but also for the development of nuclear fusion energy [1]. According to the types of irradiation particles, irradiation can be divided into neutron irradiation and ion irradiation. Neutron irradiation can offer the irradiation conditions that are close to the real environment of nuclear fission and fusion reactors. However, due to the limitations of neutron irradiation experiments, such as the limited irradiation sources, high radioactivity of irradiated samples, high cost and long experimental period, increasing interests have been focused on ion irradiation, which offers an effective alternative to study the fundamental mechanisms of irradiation effect [2–4]. Comparing with neutron irradiation, the execution of ion irradiation experiments has many advantages, namely, sufficient ion irradiation sources, low radioactivity, cheap costs and short experimental period [5,6]. Whereas, given the limited irradiation depth (usually within tens of microns) and non-uniformly distributed irradiation defects under ion irradiation, it is generally difficult to characterize the mechanical properties of ion-irradiated materials by traditional mechanical test methods [7–9]. In recent years nanoindentation, with the advantage of sample preparation and plenty of experimental data offered within a limited time, has been widely considered for the hardness measurement of ion-irradiated materials [10,11].

It is well known that ion irradiation can significantly lead to the increase of materials hardness due to the impediment of sliding dislocations by irradiation damage [12–14]. Several models have been proposed to interpret the experimental data, and explore the fundamental mechanisms related to the depth-dependent hardness of ion-irradiated materials [15–22]. Thereinto, Nix-Gao model [18] is one of the most widely applied theoretical models that initially explained the indentation size effect (ISE) of unirradiated materials by introducing the concept of geometrically necessary dislocations (GNDs) [23]. Based on the Nix-Gao model, the square of the indentation hardness is noticed to increase linearly with the

* Corresponding author.
** Corresponding author.
E-mail addresses: xxz2017@csu.edu.cn (X. Xiao), jiangc@hnu.edu.cn (C. Jiang).

https://doi.org/10.1016/j.net.2021.03.007

inverse of the indentation depth. This relationship agrees well with many nanoindentation results, and leads to the development of the mechanism-based strain gradient plasticity theory [18]. However, this model does not cover any information about irradiation-induced defects within the irradiated layer, therefore, the fundamental mechanisms of irradiation hardening cannot be well characterized. The Orowan model [19] can effectively address the contribution of irradiation defects to hardness. However, strictly speaking, it is applicable only when the defect distribution is uniform. Therefore, in order to effectively evaluate the damage gradient effect caused by non-uniform distribution of ion-irradiated defects, the average defect distribution [16] and average defect density within the plastic zone [15] were considered to revise the Orowan model [19]. Very recently, Xiao et al. [20,22] established a mechanistic model addressing the depth-dependent hardness of ion-irradiated materials by surface nanoindentation. The model is capable of capturing the ISE, ion irradiation-induced damage gradient effect and softening effect of the unirradiated substrate. The rationality and accuracy of the model have been effectively verified by comparing with the experimental data of ion-irradiated stainless steel.

On the other hand, previous literatures have indicated that the grain size plays an important role in determining the strength of unirradiated polycrystalline materials [24–29]. According to the classic Hall-Petch relationship, the yield strength of bulk materials (σ_y) as a function of the average grain size d can be expressed as $\sigma_y = \sigma_0 + K_y/d$ [25], where σ_0 is the friction stress, and K_y is the macroscopic Hall-Petch coefficient, which represents the accumulated strengthening effect of the grain boundaries. Whereas, in spite of the extensive effort, there still exist some limitations for the existing models, especially for the hardness characterization of ion-irradiated polycrystals with grain size effect. Experimental investigations have indicated that (1) the materials hardness of both unirradiated and ion-irradiated polycrystals increases with decreasing grain size, which is known as the Hall-Petch relationship [30–35]; (2) smaller grain size gives rise to less irradiation hardening for ion-irradiated materials [32,34]. However, to the authors' knowledge, the effects of grain size and ion irradiation have not been simultaneously addressed in the existing irradiation hardening analysis models.

In order to further investigate the hardening mechanisms of ion-irradiated polycrystals, two general models, i.e. the linear and square superposition models with both irradiation and grain size effects, are proposed in this work for the depth-dependent hardness of ion-irradiated polycrystals. The paper is organized as follows. Section 2 introduces the detailed derivation of the two models. Section 3 provides a simple approach for the effective fitting of model parameters based on the hardness data. The rationality of these two models is analyzed by comparing the theoretical results with several different sets of experimental data in Section 4. Finally, the corresponding conclusions are drawn in Section 5.

2. Model development

To begin with, we first consider the nanoindentation of ion-irradiated polycrystals, as illustrated in Fig. 1. During the indentation process, a plastic zone (the region where the resolved shear stress is greater than the critical resolved shear stress (CRSS), and is generally assumed as a hemisphere) is formed beneath the indenter tip. Within the plastic zone, the sliding of dislocations is

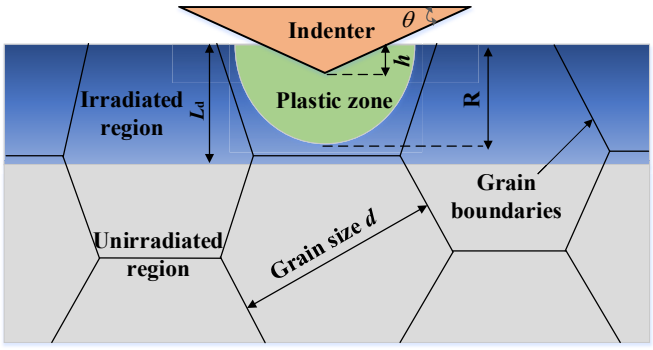

Fig. 1. A schematic diagram for the surface nanoindentation of ion-irradiated polycrystals. The irradiation depth is L_d, and the plastic zone is assumed as a hemisphere with radius R. d and h, respectively, indicate the mean grain size and indentation depth. θ characterizes the geometrical configuration of the indenter tip.

impeded by network dislocations, irradiation-induced defects and existing grain boundaries. According to the Taylor's dislocation model [36,37], CRSS related to the dislocation density can be generalized as

$$\tau_{\mathrm{CRSS}}^{\mathrm{dis}} \propto \mu b \sqrt{\rho} \tag{1}$$

where μ and b are the shear modulus and magnitude of Burgers vector, respectively. ρ denotes the total density of dislocation barriers. By further following the work of Nix and Gao [18], $\tau_{\mathrm{CRSS}}^{\mathrm{dis}}$ can then be recast as

$$\tau_{\mathrm{CRSS}}^{\mathrm{dis}} = \mu b \alpha \sqrt{\overline{\rho}_{\mathrm{S}} + \overline{\rho}_{\mathrm{G}}} \tag{2}$$

where α is the hardening coefficient of dislocations, $\overline{\rho}_{\mathrm{S}}$ and $\overline{\rho}_{\mathrm{G}}$ refer to, respectively, the average density of statistically stored dislocations (SSDs) [38] and GNDs [23] within the plastic zone. In general, the SSD density is related to the bulk hardness of the materials without grain size effect, and is usually a few orders of magnitude smaller than that of GNDs, especially when the indentation depth is shallow [38]. The respective expressions of $\overline{\rho}_{\mathrm{S}}$ and $\overline{\rho}_{\mathrm{G}}$ follow as

$$\begin{cases} \overline{\rho}_{\mathrm{G}} = \dfrac{3}{2b \tan\theta M^3 h} \\ \overline{\rho}_{\mathrm{S}} = \dfrac{3}{2b \tan\theta h^*} \end{cases} \tag{3}$$

where θ characterizes the geometrical configuration of the indenter tip, which affects the dislocation density during the nanoindentation process. M is the proportional coefficient that is generally taken as a constant (ranging from 5 to 10) for the concerned materials, which can be measured by experimental observations or finite element simulations [20,39,40]. For polycrystalline materials with comparatively large grain sizes, M can be effected by grain orientation or texture when the plastic zone mainly locates within one single crystal. h is the indentation depth. $\overline{h}^* = h^*/M^3$ with h^* the characteristic length depending on the SSD density through H_0. Here $H_0 = 3\sqrt{3}\mu b\alpha\sqrt{\overline{\rho}_{\mathrm{S}}}$ is the bulk hardness of unirradiated single crystals or polycrystals with large grain sizes that is determined by the density of SSDs alone [18]. After materials annealing, the initial value of SSD density may be changed that

results in the variation of H_0 to some extent. Whereas, its influence on the depth dependent hardness is limited as it is dominated by the variation of GND density with indentation depth. Finally, by substituting Eq. (3) into Eq. (2), the ultimate expression of τ_{CRSS}^{dis} yields as

$$\tau_{CRSS}^{dis} = \mu b \alpha \sqrt{\frac{3}{2b \tan\theta h^*}\left(1+\frac{\overline{h}^*}{h}\right)} \tag{4}$$

Under exposure to high energy particles, numbers of microscopic defects (e.g. dislocation loops, stacking fault tetrahedra and bubbles) are generated in the irradiated materials. These irradiation-induced defects act as barriers for the motion of dislocations. Consequently, the yield strength of irradiated materials increases [16]. Then, the CRSS related to the additional defects generated by irradiation can be written as [20].

$$\tau_{CRSS}^{def} = \mu b \beta \sqrt{\overline{N}_{def} d_{def}} \tag{5}$$

where β denotes the irradiation-induced defect hardening coefficient. $\overline{N}_{def}$ and d_{def} are respectively the average density and size of irradiation-induced defects. Moreover, $\overline{N}_{def}$ is defined as

$$\overline{N}_{def} = \int_{V_p} N_{def} dV / V_p \tag{6}$$

where V_p is the volume of the plastic zone, and the density of the ion-irradiation induced defects N_{def} is assumed to obey the following relation [20].

$$N_{def}(x) = \begin{cases} N_{def}^0 \left(\dfrac{x}{L_d}\right)^n & (x \le L_d) \\ 0 & (x > L_d) \end{cases} \tag{7}$$

where N_{def}^0 is the peak defect number density at the maximum irradiation depth. L_d and n are parameters describing the distribution profile of defects. Though expressed in an approximated form, Eq. (7) has been verified in previous literatures that it can effectively characterize the irradiation hardening behavior of ion-irradiated materials with inhomogeneously distributed defects [20–22]. By substituting Eq. (7) into Eq. (6), the average defect density in the plastic zone at different indentation depths can be obtained

$$\overline{N}_{def}(h) = \begin{cases} \dfrac{3N_{def}^0 h^n}{(n+1)(n+3)\left(h_c^{sep}\right)^n} & (h \le h_c^{sep}) \\ \dfrac{3N_{def}^0}{2}\left[\dfrac{1}{n+1}\dfrac{h_c^{sep}}{h} - \dfrac{1}{n+3}\left(\dfrac{h_c^{sep}}{h}\right)^3\right] & (h > h_c^{sep}) \end{cases} \tag{8}$$

where $h_c^{sep} = L_d/M$ is the critical indentation depth at which the plastic zone reaches the boundary $x = L_d$. Substituting Eq. (8) into Eq. (5), the ultimate expression of τ_{CRSS}^{def} yields as

$$\tau_{CRSS}^{def} = \mu b \beta \sqrt{\overline{N}_{def} d_{def}} = \begin{cases} \mu b \beta \sqrt{\dfrac{3N_{def}^0 d_{def} h^n}{(n+1)(n+3)\left(h_c^{sep}\right)^n}} (h \le h_c^{sep}) \\ \mu b \beta \sqrt{\dfrac{3N_{def}^0 d_{def}}{2}\left[\dfrac{1}{n+1}\dfrac{h_c^{sep}}{h} - \dfrac{1}{n+3}\left(\dfrac{h_c^{sep}}{h}\right)^3\right]} (h > h_c^{sep}) \end{cases} \tag{9}$$

Besides the hardening contribution induced by network dislocation interaction and dislocation-defect interaction, there also exists another critical hardening mechanism for ion-irradiated polycrystals, i.e. the Hall-Petch effect related to the impediment of sliding dislocations by grain boundaries [30–35]. Following the Hall-Petch relationship [24], the CRSS affected by grain boundaries can be expressed as

$$\tau_{CRSS}^{hp} = \frac{k_{hp}}{\sqrt{d}} \tag{10}$$

where k_{hp} is the Hall-Petch coefficient. Finally, in order to deduce the expression of CRSS containing all the three dominant hardening mechanisms, i.e. τ_{CRSS}^{dis}, τ_{CRSS}^{def} and τ_{CRSS}^{hp}, one may consider either the linear superposition model (or say Model I) or square superposition model (or say Model II), i.e.

$$\tau_{CRSS}^{irr} = \begin{cases} \tau_{CRSS}^{dis} + \tau_{CRSS}^{def} + \tau_{CRSS}^{hp} & \text{Model I} \\ \sqrt{\left(\tau_{CRSS}^{dis}\right)^2 + \left(\tau_{CRSS}^{def}\right)^2 + \left(\tau_{CRSS}^{hp}\right)^2} & \text{Model II} \end{cases} \tag{11}$$

By further considering the Mises flow rule [41] and Tabor's factor [42], the hardness model of ion-irradiated polycrystals can, therefore, be deduced as

$$H_{\mathrm{irr}}=3\sqrt{3}\tau_{\mathrm{CRSS}}^{\mathrm{irr}}=\begin{cases}H_0\left[\sqrt{1+\dfrac{\overline{h}^*}{h}}+\sqrt{\dfrac{A^2\overline{h}^*h^n}{(n+1)(n+3)\left(h_{\mathrm{c}}^{\mathrm{sep}}\right)^{n+1}}}+\sqrt{\dfrac{K}{d}}\right]\left(h\le h_{\mathrm{c}}^{\mathrm{sep}}\right) & \text{Model I}\\ H_0\sqrt{1+\dfrac{\overline{h}^*}{h}+\dfrac{A^2\overline{h}^*h^n}{(n+1)(n+3)\left(h_{\mathrm{c}}^{\mathrm{sep}}\right)^{n+1}}+\dfrac{K}{d}}\left(h\le h_{\mathrm{c}}^{\mathrm{sep}}\right) & \text{Model II}\end{cases}\tag{12}$$

and

$$H_{\mathrm{irr}}=\begin{cases}H_0\left[\sqrt{1+\dfrac{\overline{h}^*}{h}}+\sqrt{\dfrac{A^2\overline{h}^*}{2h}\left[\dfrac{1}{n+1}-\dfrac{\left(h_{\mathrm{c}}^{\mathrm{sep}}\right)^2}{(n+3)h^2}\right]}+\sqrt{\dfrac{K}{d}}\right]\left(h>h_{\mathrm{c}}^{\mathrm{sep}}\right) & \text{Model I}\\ H_0\sqrt{1+\dfrac{\overline{h}^*}{h}+\dfrac{A^2\overline{h}^*}{2h}\left[\dfrac{1}{n+1}-\dfrac{\left(h_{\mathrm{c}}^{\mathrm{sep}}\right)^2}{(n+3)h^2}\right]+\dfrac{K}{d}}\left(h>h_{\mathrm{c}}^{\mathrm{sep}}\right) & \text{Model II}\end{cases}\tag{13}$$

where $K=27k_{\mathrm{hp}}^2/H_0^2$ and $A=\beta/\alpha M\sqrt{2b\tan\theta L_{\mathrm{d}}N_{\mathrm{def}}^0d_{\mathrm{def}}}$. As indicated in Eqs. (12) and (13), three distinguishing hardening mechanisms are characterized in the proposed hardness model. Besides the depth-dependent dislocation and defect hardening mechanisms (the first two terms on the right hand of Eqs. (12) and (13)), the hardening contribution induced by grain boundaries is addressed to characterize the dependence of materials hardness on grain size. This hardening mechanism can be obviously noticed when the grain size of polycrystals decreases down to hundreds of nanometers [30–35], as observed in the previous experimental work that the hardness of ion-irradiated Fe–14Cr-based alloys increases when the grain size decreases from 1.15 μm to 0.32 μm. In this case, the parameter H_0 fitted by the previous models varies with the grain size, which makes the physical interpretation of H_0 become questionable. This also indicates the necessity of establishing a hardening model that is able to address grain size effect for ion-irradiated polycrystals. Futhermore, the proposed model can be deduced to either the Nix-Gao model [18] when both irradiation and grain size effect are ignored, or the Xiao's model [22] when the grain size effect is relatively weak. When interpreting the grain size dependence of the hardness of unirradiated polycrystals, one can also have

$$H_{\mathrm{uni}}=\begin{cases}H_0\left(\sqrt{1+\dfrac{\overline{h}^*}{h}}+\sqrt{\dfrac{K}{d}}\right) & \text{Model I}\\ H_0\sqrt{1+\dfrac{\overline{h}^*}{h}+\dfrac{K}{d}} & \text{Model II}\end{cases}\tag{14}$$

which ignores the hardening contribution induced by irradiation-induced defects.

Strictly speaking, both Model I and II in Eq. (13) are limited to polycrystalline materials as the dominant purpose of this work is to develop a theoretical model covering both irradiation and grain size effect. When the grain size decreases below 100 nm (nanocrystals), the contribution of grain boundaries to the macroscopic materials properties tends to become dominant, and corresponding formula characterizing the grain boundary behavior should be addressed, then, Eq. (13) for polycrtstalline materials may no longer hold. On the contrary, when the grain size becomes much larger than the indentation depth, the grain boundary effect is limited, and the developed model in Eq. (13) can then be applicable for single crystals by ignoring the last Hall-Petch term $H_0\sqrt{K/d}$.

3. Model parameter calibration

In order to calibrate the hardness model as expressed in Eqs. (12) and (13), one can divide the parameters into two groups, including the ones without irradiation effect, i.e. H_0, K and $\overline{h}^*$, and the ones affected by ion irradiation, i.e. n,A and $h_{\mathrm{c}}^{\mathrm{sep}}$. For the former three parameters without irradiation effect, H_0 and K are unaffected by the grain size, while the decrease of grain size could limit the expansion of the plastic zone, therefore, lead to the decrease of the proportional coefficient M and then the increase of $\overline{h}^*$. In the following, the parameter calibration process is given in details.

Firstly, after the conduction of indentation tests on unirradiated polycrystals with two different grain sizes, i.e. d_1 and d_2, it is available to obtain two experimental $H_{\mathrm{uni}}^{\mathrm{exp}}\sim h$ curves. Then, the difference between the experimental data and theoretical results (say Model I for instance) at the i-th indentation depth can be calculated as

$$\begin{cases}\Delta H_1(i)=H_{\mathrm{uni1}}^{\mathrm{exp}}(i)-H_{\mathrm{uni1}}^{\mathrm{theory}}(i)=H_{\mathrm{uni1}}^{\mathrm{exp}}(i)-H_0\left[\sqrt{1+\dfrac{\overline{h}_1^*}{h(i)}}+\sqrt{\dfrac{K}{d_1}}\right]\\ \Delta H_2(i)=H_{\mathrm{uni2}}^{\mathrm{exp}}(i)-H_{\mathrm{uni2}}^{\mathrm{theory}}(i)=H_{\mathrm{uni2}}^{\mathrm{exp}}(i)-H_0\left[\sqrt{1+\dfrac{\overline{h}_2^*}{h(i)}}+\sqrt{\dfrac{K}{d_2}}\right]\end{cases}\tag{15}$$

where $\overline{h}_1^*$ and $\overline{h}_2^*$ are corresponding to the grain size d_1 and d_2.

Table 1
Parameters of Model I and Model II for unirradiated polycrystalline Cu with different grain sizes.

	Model I		Model II	
d (μm)	0.90	1.15	0.90	1.15
$\overline{h}^*$ (μm)	2.07	1.78	4.80	4.67
H_0 (GPa)	0.59		0.49	
K (μm)	0.71		3.93	
k_{hp} (MPa$\sqrt{m}$)	0.10		0.19	

Table 2
Parameters of Model I and Model II for unirradiated Fe–14Cr-based alloys with different grain sizes.

	Model I		Model II	
d (μm)	0.32	1.15	0.32	1.15
$\overline{h}^*$ (μm)	4.16	3.53	2.21	1.71
M(−)	10	14.3	7.7	10
H_0 (GPa)	0.18		0.50	
α (−)	0.2		0.4	
K (μm)	77.36		13.22	
k_{hp} (MPa$\sqrt{m}$)	0.31		0.35	

Table 3
Parameters of Model I and Model II for the ion-irradiated Fe–14Cr-based alloys with different grain sizes.

	Model I		Model II	
d (μm)	0.32	1.15	0.32	1.15
T (μm)	1.37	5.82	3.72	5.10
$Z\cdot$ (μm^3)	9.02E-3	1.87E-3	0.03	0.03
n 2.39	2.51	0.85	1.17	
p(um^{-n})	1.14E3	2.25E4	85.18	361.20
h_c^{sep}(um)	0.10	0.07	0.13	0.10
β(−)	0.2		0.6	
A(−)	1.49	3.40	2.50	3.59

Table 4
Parameters of Nix-Gao model for unirradiated polycrystalline Cu with different grain sizes.

d (μm)	0.9	1.15
H_0 (GPa)	1.14	1.03
$\overline{h}^*$ (μm)	0.87	1.09

When further applying the genetic algorithm [43], one can simultaneously obtain H_0,$\overline{h}_1^*$, $\overline{h}_2^*$ and K by solving the minimum sum of $\sum_i[\Delta H_1^2(i)+\Delta H_2^2(i)]$. The same calibration process also works for Model II in order to obtain the set of H_0,$\overline{h}_1^*$, $\overline{h}_2^*$ and K for unirradiated polycrystalline samples with different grain sizes. Once H_0 is obtained, the value of α can be calculated through $\alpha = H_0/(3\sqrt{3}\mu b\sqrt{\overline{\rho}_S})$ with μ, b and $\overline{\rho}_S$ measured or informed in the literature.

Next, in order to calibrate the rest irradiation-dependent parameters, i.e. n, A and h_c^{sep}, one needs to conduct indentation tests on the ion-irradiated sample with a given grain size (d_1 or d_2), which yields the $H_{irr}^{exp} \sim h$ curves with irradiation effect. Given the calibrated value of H_0, $\overline{h}^*$ and K in the previous step, one may transform the $H_{irr}^{exp} \sim h$ curves into the form as

$$f_{exp}(h) = \begin{cases} \left(\frac{H_{irr}^{exp}}{H_0} - \sqrt{\frac{\overline{h}^*}{h}+1} - \sqrt{\frac{K}{d}}\right)^2 & \text{Model I} \\ \left(\frac{H_{irr}^{exp}}{H_0}\right)^2 - \frac{\overline{h}^*}{h} - 1 - \frac{K}{d} & \text{Model II} \end{cases} \quad (16)$$

where one should note that the parameter K is assumed to keep the same before and after irradiation given the irradiation-induced defects may have limited effect on the properties of grain boundaries. Otherwise, the model can hardly be applied to the irradiated samples with varying defect density and grain size at the same time. Similarly, the theoretical model expressed in Eqs. (12) and (13) can be deduced as

$$f(h) = \begin{cases} Ph^n (h \le h_c^{sep}) \\ \frac{T}{h} - \frac{Z}{h^3} (h > h_c^{sep}) \end{cases} \quad (17)$$

where $P = A^2\overline{h}^*/[(n+1)(n+3)(h_c^{sep})^{n+1}]$,$T = P/2(n+3)(h_c^{sep})^{n+1}$ and $Z = P/2(n+1)(h_c^{sep})^{n+3}$. By comparing the theoretical relationship $f(h)$ with the experimental data $f_{exp}(h)$, the determination of parameters n, P, T, Z, h_c^{sep}, and A can be performed following the calibration process as detailed in Ref. [20]. Furthermore, the values of M and β can then be, respectively, obtained by $M = L_d/h_c^{sep}$ and $\beta = A\alpha/(M\sqrt{2b\tan\theta L_d N_{def}^0 d_{def}})$ with corresponding irradiation related information (L_d, N_{def}^0 and d_{def}) measured in the ion irradiation experiments.

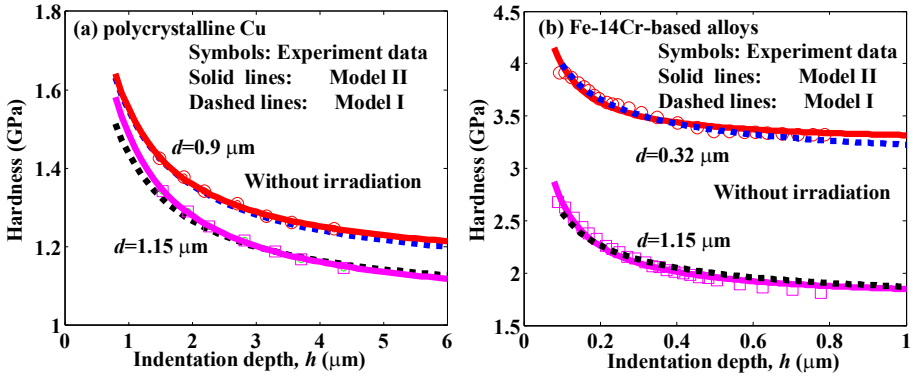

Fig. 2. Hardness-depth relationships with grain size effect compared between Model I and II with unirradiated experimental data of (a) polycrystalline Cu [18], and (b) Fe–14Cr-based alloys [15].

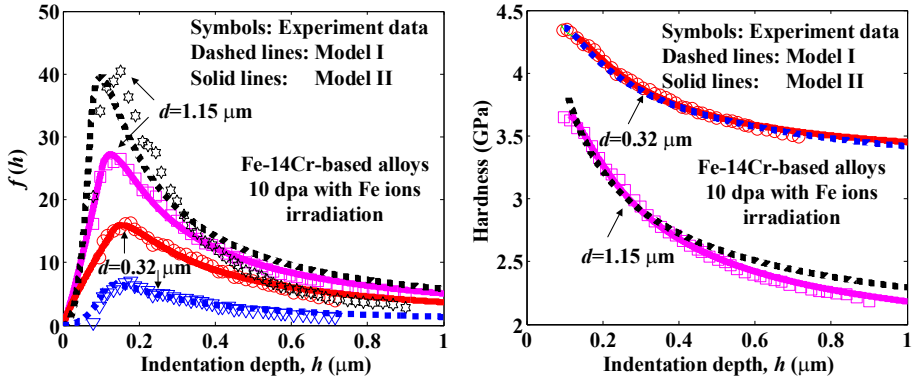

Fig. 3. (a) $f(h) - h$ and (b) hardness-depth relationship with grain size effect compared between Model I and II with ion-irradiated experimental data of Fe–14Cr-based alloys [15].

4. Model validation and discussion

In this section, two sets of experimental data are adopted to compare with Model I and II, including unirradiated polycrystalline copper with grain size of 0.9 μm and 1.15 μm [30], and ion-irradiated Fe–14Cr-based alloys with grain size of 0.32 μm and 1.15 μm [34]. The main purpose of this comparison is not only to verify the rationality of the proposed models, but also to help evaluate which one works better for the hardness characterization of ion-irradiated polycrystals with both irradiation and grain size effects. Following the above mentioned parameter calibration process, the parameters for Model I and II are collected in Tables 1, 2 and 3. In addition, the parameters fitted by the Nix-Gao model for unirradiated polycrystalline copper are also collected in Table 4 as a comparison, which indicate unreasonable high bulk hardness values for unirradiated polycrystalline copper.

Fig. 2 compares the unirradiated experimental data of polycrystalline copper and Fe–14Cr-based alloys with the theoretical results of Model I and II (as expressed in Eq. (14)), which noteworthily indicates that: (1) Both Model I and II could effectively characterize the ISE and grain size effect of unirradiated polycrystals, and both of them match well with the experimental data. (2) The fitted parameters H_0, K and further deduced parameter $k_{hp} = H_0\sqrt{K}$ of Model I and II are independent of grain size, and seem reasonable as they are close to the literature values [30], i.e. $H_0 = 0.55$ GPa and $k_{hp} = 0.14$ MPa$\sqrt{\text{m}}$. Whereas, $\overline{h}^* = h^*/M^3$ is noticed to decrease with the increase of grain size. Given that the decrease of grain size could to some extent inhibit the expansion of the plastic zone due to the impediment of sliding dislocations by grain boundaries, therefore, M tends to decrease with the grain size, which finally results in the increase of $\overline{h}^*$ at small grain sizes. By comparing with the Nix-Gao model, an obvious advantage of the model developed in this work is that one can simultaneously obtain H_0 and k_{hp} by separating the grain size effect from the dislocation hardening contribution. More importantly, the fitted parameter H_0 is much closer to the experimental data and the physical meaning is more rational.

In addition, Fig. 3 illustrates the $f(h) - h$ and hardness-depth relationship with both irradiation and grain size effects, which are compared between Model I and II with the experimental data of ion-irradiated Fe–14Cr-based alloys [34]. The irradiation dose is 10 dpa. Please note that for a given grain size, the transformed experimental $f - h$ relation may not be the same for Model I and II, as both the model expression and parameters (e.g. $\overline{h}^*$) are different. It can be seen that: (1) The transformed experimental data given in Fig. 3(a) can effectively represent the inhomogeneously distributed irradiation hardening behavior of ion-irradiated materials. Irradiation hardening becomes increasingly obvious at the initial indentation depths until the plastic zone transports into the

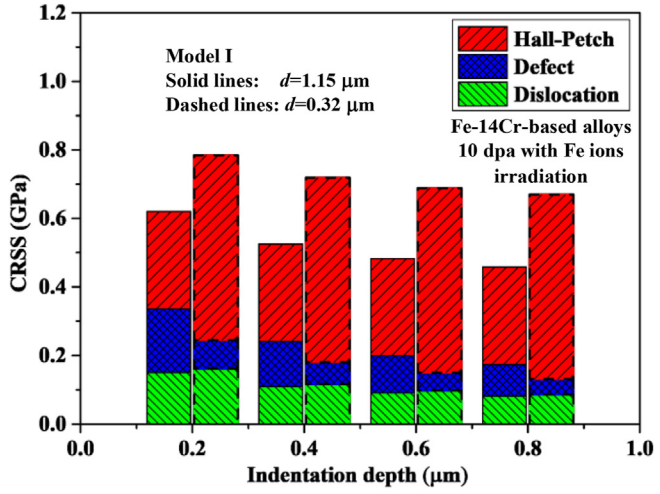

Fig. 4. Contribution of network dislocation interaction, dislocation-defect interaction and Hall-Petch effect to the critical resolved shear stress of ion-irradiated Fe–14Cr-based alloys with grain size of 0.32 μm and 1.15 μm at different indentation depths.

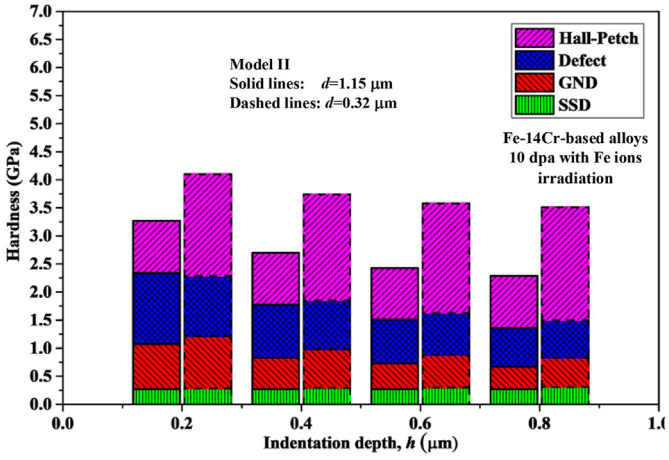

Fig. 5. Hardening contribution of SSDs, GNDs, irradiation-induced defects and grain boundaries to the indentation hardness of ion-irradiated Fe–14Cr-based alloys with grain size of 0.32 μm and 1.15 μm at different indentation depths.

unirradiated region that the substrate softening mechanism becomes dominant. (2) Irradiation hardening is more noticeable for the sample with large grain size when compared with that with small grain size. Actually, the proportion of grain boundaries tends to increase with the decrease of grain size, which offers sufficient defect sinks for the irradiation-induced point defects and helps alleviate the irradiation hardening phenomenon [31,33,34]. (3) The fitted values of the Hall-Petch coefficient k_{hp} at room temperature are 0.31 MPa$\sqrt{m}$ for Model I and 0.35 MPa$\sqrt{m}$ for Model II, which are close to the literature value of 0.39 MPa$\sqrt{m}$ [44]. (4) For ion-irradiated polycrystals, Model II performs better than Model I when characterizing the hardness-depth relationship with large grain size. Considering the expression of CRSS for Model I and Model II as expressed in Eq. (11), it is not difficult to approximately have the additional increment terms $\sqrt{2\tau_{CRSS}^{def}\tau_{CRSS}^{hp}}$, $\sqrt{2\tau_{CRSS}^{dis}\tau_{CRSS}^{hp}}$, $\sqrt{2\tau_{CRSS}^{def}\tau_{CRSS}^{dis}}$ for Model I when compared with Model II. As shown in Fig. 4, for the fine grain, τ_{CRSS}^{hp} is much larger than τ_{CRSS}^{dis} and τ_{CRSS}^{def} during the nanoindentation process, therefore, these additional increment terms can be ignored when comparing with τ_{CRSS}^{irr} respectively given in Model I and Model II. However, for the coarse grain, the magnitude of τ_{CRSS}^{hp}, τ_{CRSS}^{def} and τ_{CRSS}^{dis} gets much closer. Consequently, the additional increment terms can be obviously noticed, and make the results of Model I deviate from the experimental data. This also implies that it is more rational to apply Model II for the hardness characterization of ion-irradiated polycrystals.

After the calibration of model parameters, we have categorized the parameters into two groups, including the ones with and without irradiation effect, as listed in Tables 2 and 3. It is then available to further verify the rationality and accuracy of the proposed model by comparing some intrinsic materials parameters with the literature values. For instance, M can be calculated by $M = L_d/h_c^{sep}$ under ion irradiation conditions. In this work, the irradiation depth is 1 μm [34], and h_c^{sep} has been calibrated as given in Table 2. Then, the M-values with different grain sizes for ion-irradiated Fe−14Cr alloys can be obtained for the two models (Table 2). It can be seen that the M-values are 10 and 14.3 for Model I when the grain sizes are 0.32 μm and 1.15 μm, respectively. As a comparison, the M-values range from 7.7 to 10 for Model II, which are closer to the literature values (from 5 to 10) [20,39,40]. These numerical results further indicate that Model II performs better than Model I under irradiation conditions. In addition, the hardening coefficients, α and β, can also be calculated for the ion-irradiated Fe−14Cr alloys. Thereinto, α is obtained from $\alpha = H_0/(3\sqrt{3}\,\mu b\sqrt{\overline{\rho}_S})$ with $\mu = 84$ GPa, $b = 2.48E-10$ m and $\overline{\rho}_S = 9.7E13$ m^{-2} [45]. Moreover, β can be calculated through $\beta = A\alpha/(M\sqrt{2b\tan\theta L_d N_{def}^0 d_{def}})$ with $b = 2.48E-10$ m, $\tan\theta = 0.3579$, $L_d = 1$ μm, $N_0^{def} = 25E22$ m^{-3} and $d_{def} = 1.1E-10$ m [34,45]. As summarized in Table 2, one can see that α equals 0.2 and 0.4 for Model I and II, respectively, which seems reasonable as they are close to the literature value, i.e. $\alpha = 0.33$ [45]. As a comparison, β equals 0.2 for Model I and 0.6 for Model II. Given that the literature value of β is 0.63 [46], then one may again verify the dominant conclusion of this work that Model II performs better than Model I when addressing the hardness of ion-irradiated polycrystals with obvious grain size effect, i.e. the hardening contribution of grain boundaries is comparable with both the dislocation and defect hardening contribution for the overall hardness.

Furthermore, the proposed model offers an effective method to evaluate the contribution of different hardening mechanisms to the materials hardness. Take Model II with calibrated parameters for an instance, Fig. 5 compares the hardening contribution of GNDs, SSDs, irradiation-induced defects and grain boundaries at different indentation depths for ion-irradiated Fe−14Cr-based alloys with grain size of 0.32 μm and 1.15 μm. As one can see: (1) Besides the hardening terms of grain boundaries and SSDs, the contribution of both GNDs and irradiation-induced defects tends to decrease with increasing indentation depth. The former originates from the decrease of the density of GNDs, and the latter can be ascribed to the substrate softening effect. (2) Comparing with the sample with large grain size, the dominant hardening mechanism for the sample with small grain size is mainly determined by the Hall-Petch effect, especially at the deep indentation depth. (3) The hardening contribution of irradiation-induced defects for the sample with small grain size is lower than that with large grain size, which is consistent with the experimental data as presented in Fig. 3(a).

5. Conclusion

To conclude, a mechanistic model with grain size effect is proposed for the depth-dependent hardness of ion-irradiated polycrystals. Two submodels are deduced, including the linear and square superposition versions. Four dominant hardening mechanisms are addressed in the hardness model, i.e. the hardening contribution of GNDs, SSDs, irradiation-induced defects and grain boundaries. By comparing with the experimental data of both unirradiated and ion-irradiated polycrystals with different grain sizes, the dominant results can be summarized as follows:

(1) The new model separates the grain size effect from the dislocation hardening contribution, which makes the physical meaning of fitted parameters more rational when compared with existing hardening models.
(2) For unirradiated samples with obvious grain size effect, both linear and square superposition models can well characterize the experimental data; whereas, for ion-irradiated materials, the square superposition hardening model performs better.
(3) The square superposition hardening model is recommended to characterize the hardening behavior of both unirradiated and irradiated polycrystals with obvious grain size effect.

Declaration of competing interest

The authors declare that they have no known competing financial interests or personal relationships that could have appeared to influence the work reported in this paper.

Acknowledgement

This work was supported by the National Science Fund for Distinguished Young Scholars, China (Grant No. 51725502), the Foundation for Innovative Research Groups of the National Natural Science Foundation of China (Grant No. 51621004), the National Nature Science foundation of China (NSFC) under Contract No, 11802344, and Natural Science Foundation of Hunan Province, China (Grant No. 2019JJ50809).

References

[1] S.J. Zinkle, J.T. Busby, Structural materials for fission & fusion energy, Mater. Today 12 (11) (2009) 12–19.
[2] W.Q. Chen, X.Z. Xiao, B. Pang, S.S. Si, Y.Z. Jia, B. Xu, T.W. Morgan, W. Liu, Y.L. Chiu, Irradiation hardening induced by blistering in tungsten due to low-energy high flux hydrogen plasma exposure, J. Nucl. Mater. 522 (2019) 11–18.
[3] S.I. Kim, B.H. Kim, J.L. Kim, J.I. Lee, A review of neutron scattering correction for the calibration of neutron survey meters using the shadow cone method,

Nuclear Engineering and Technology 47 (7) (2015) 939–944.
[4] G.S. Was, Z. Jiao, E. Getto, K. Sun, A.M. Monterrosa, S.A. Maloy, O. Anderoglu, B.H. Sencer, M. Hackett, Emulation of reactor irradiation damage using ion beams, Scripta Mater. 88 (2014) 33–36.
[5] C. Heintze, F. Bergner, S. Akhmadaliev, E. Altstadt, Ion irradiation combined with nanoindentation as a screening test procedure for irradiation hardening, J. Nucl. Mater. 472 (2016) 196–205.
[6] R. Kasada, S. Konishi, K. Yabuuchi, S. Nogami, M. Ando, D. Hamaguchi, H. Tanigawa, Depth-dependent nanoindentation hardness of reduced-activation ferritic steels after MeV Fe-ion irradiation, Fusion Eng. Des. 89 (7) (2014) 1637–1641.
[7] Z. Fan, S. Zhao, K. Jin, D. Chen, Y.N. Osetskiy, Y. Wang, H. Bei, K.L. More, Y. Zhang, Helium irradiated cavity formation and defect energetics in Ni-based binary single-phase concentrated solid solution alloys, Acta Mater. 164 (2019) 283–292.
[8] C.D. Hardie, S.G. Roberts, A.J. Bushby, Understanding the effects of ion irradiation using nanoindentation techniques, J. Nucl. Mater. 462 (2015) 391–401.
[9] P. Sun, Y. Wang, M. Frost, C. Schönwälder, A.L. Levitan, M. Mo, Z. Chen, J.B. Hastings, G.R. Tynan, S.H. Glenzer, P. Heimann, Characterization of defect clusters in ion-irradiated tungsten by X-Ray diffuse scattering, J. Nucl. Mater. 510 (2018) 322–330.
[10] A. Prasitthipayong, S.J. Vachhani, S.J. Tumey, A.M. Minor, P. Hosemann, Indentation size effect in unirradiated and ion-irradiated 800H steel at high temperatures, Acta Mater. 144 (2018) 896–904.
[11] C. Xu, L. Zhang, W. Qian, J. Mei, X. Liu, The studies of irradiation hardening of stainless steel reactor internals under proton and xenon irradiation, Nuclear Engineering and Technology 48 (3) (2016) 758–764.
[12] C. Heintze, F. Bergner, M. Hernández-Mayoral, Ion-irradiation-induced damage in Fe–Cr alloys characterized by nanoindentation, J. Nucl. Mater. 417 (1) (2011) 980–983.
[13] X. Xiao, L. Chen, L. Yu, H. Duan, Modelling nano-indentation of ion-irradiated FCC single crystals by strain-gradient crystal plasticity theory, Int. J. Plast. 116 (2019) 216–231.
[14] C. Yan, R. Wang, Y. Wang, X. Wang, G. Bai, Effects of ion irradiation on microstructure and properties of zirconium alloys—a review, Nuclear Engineering and Technology 47 (3) (2015) 323–331.
[15] D. Chen, K. Murakami, K. Dohi, K. Nishida, N. Soneda, Z. Li, L. Liu, N. Sekimura, Depth distribution of Frank loop defects formed in ion-irradiated stainless steel and its dependence on Si addition, Nucl. Instrum. Methods Phys. Res. Sect. B Beam Interact. Mater. Atoms 365 (2015) 503–508.
[16] Z.Y. Fu, P.P. Liu, F.R. Wan, Q. Zhan, Helium and hydrogen irradiation induced hardening in CLAM steel, Fusion Eng. Des. 91 (2015) 73–78.
[17] Y. Huang, F. Zhang, K.C. Hwang, W.D. Nix, G.M. Pharr, G. Feng, A model of size effects in nano-indentation, J. Mech. Phys. Solid. 54 (8) (2006) 1668–1686.
[18] W.D. Nix, H. Gao, Indentation size effects in crystalline materials: a law for strain gradient plasticity, J. Mech. Phys. Solid. 46 (3) (1998) 411–425.
[19] E. Orowan, A type of plastic deformation new in metals, Nature 149 (3788) (1942) 643–644.
[20] X. Xiao, Q. Chen, H. Yang, H. Duan, J. Qu, A mechanistic model for depth-dependent hardness of ion irradiated metals, J. Nucl. Mater. 485 (2017) 80–89.
[21] X. Xiao, L. Yu, A hardening model for the cross-sectional nanoindentation of ion-irradiated materials, J. Nucl. Mater. 511 (2018) 220–230.
[22] X. Xiao, L. Yu, Comparison of linear and square superposition hardening models for the surface nanoindentation of ion-irradiated materials, J. Nucl. Mater. 503 (2018) 110–115.
[23] J.F. Nye, Some geometrical relations in dislocated crystals, Acta Metall. 1 (2) (1953) 153–162.
[24] G.J. Weng, A micromechanical theory of grain-size dependence in metal plasticity, J. Mech. Phys. Solid. 31 (3) (1983) 193–203.
[25] E.O. Hall, The deformation and ageing of mild steel: III discussion of results, Proc. Phys. Soc. B 64 (9) (1951) 747–753.
[26] A. Singh, Y. Osawa, H. Somekawa, T. Mukai, Effect of microstructure on strength and ductility of high strength quasicrystal phase dispersed Mg–Zn–Y alloys, Mater. Sci. Eng., A 611 (2014) 242–251.
[27] Y. Wang, H. Choo, Influence of texture on Hall–Petch relationships in an Mg alloy, Acta Mater. 81 (2014) 83–97.
[28] H. Yu, Y. Xin, M. Wang, Q. Liu, Hall-Petch relationship in Mg alloys: a review, J. Mater. Sci. Technol. 34 (2) (2018) 248–256.
[29] B. Guan, Y. Xin, X. Huang, P. Wu, Q. Liu, Quantitative prediction of texture effect on Hall–Petch slope for magnesium alloys, Acta Mater. 173 (2019) 142–152.
[30] X. Hou, N.M. Jennett, Application of a modified slip-distance theory to the indentation of single-crystal and polycrystalline copper to model the interactions between indentation size and structure size effects, Acta Mater. 60 (10) (2012) 4128–4135.
[31] Y. Ha, A. Kimura, Effect of recrystallization on ion-irradiation hardening and microstructural changes in 15Cr-ODS steel, Nucl. Instrum. Methods Phys. Res. Sect. B Beam Interact. Mater. Atoms 365 (2015) 313–318.
[32] G.M. Cheng, W.Z. Xu, Y.Q. Wang, A. Misra, Y.T. Zhu, Grain size effect on radiation tolerance of nanocrystalline Mo, Scripta Mater. 123 (2016) 90–94.
[33] E. Hug, R. Prasath Babu, I. Monnet, A. Etienne, F. Moisy, V. Pralong, N. Enikeev, M. Abramova, X. Sauvage, B. Radiguet, Impact of the nanostructuration on the corrosion resistance and hardness of irradiated 316 austenitic stainless steels, Appl. Surf. Sci. 392 (2017) 1026–1035.
[34] C. Heintze, I. Hilger, F. Bergner, T. Weissgärber, B. Kieback, Nanoindentation of single- (Fe) and dual-beam (Fe and He) ion-irradiated ODS Fe-14Cr-based alloys: effect of the initial microstructure on irradiation-induced hardening, J. Nucl. Mater. 518 (2019) 1–10.
[35] G. Monnet, C. Mai, Prediction of irradiation hardening in austenitic stainless steels: analytical and crystal plasticity studies, J. Nucl. Mater. 518 (2019) 316–325.
[36] G.I. Taylor, The mechanism of plastic deformation of crystals. Part I. Theoretical, Proc. Roy. Soc. Lond. 145 (855) (1934) 362–387.
[37] G.I. Taylor, Plastic strain in metals, J. Inst. Met. 62 (1938) 307–324.
[38] M. Ashby, The deformation of plastically non-homogeneous materials, Phil. Mag.: A Journal of Theoretical Experimental and Applied Physics 21 (170) (1970) 399–424.
[39] T. Miura, K. Fujii, K. Fukuya, K. Takashima, Influence of crystal orientation on hardness and nanoindentation deformation in ion-irradiated stainless steels, J. Nucl. Mater. 417 (1–3) (2011) 984–987.
[40] H. Huang, J. Li, D. Li, R. Liu, G. Lei, Q. Huang, L. Yan, TEM, XRD and nanoindentation characterization of Xenon ion irradiation damage in austenitic stainless steels, J. Nucl. Mater. 454 (1–3) (2014) 168–172.
[41] A.L. Gurson, Continuum Theory of Ductile Rupture by Void Nucleation and Growth: Part I—Yield Criteria and Flow Rules for Porous Ductile Media, 1977.
[42] D. Tabor, A simple theory of static and dynamic hardness, Proc. Roy. Soc. Lond. Math. Phys. Sci. 192 (1029) (1948) 247–274.
[43] D. Whitley, A genetic algorithm tutorial, Stat. Comput. 4 (2) (1994) 65–85.
[44] X. Xiao, D. Terentyev, L. Yu, A. Bakaev, Z. Jin, H. Duan, Investigation of the thermo-mechanical behavior of neutron-irradiated Fe-Cr alloys by self-consistent plasticity theory, J. Nucl. Mater. 477 (2016) 123–133.
[45] M. Dadé, J. Malaplate, J. Garnier, F. De Geuser, F. Barcelo, P. Wident, A. Deschamps, Influence of microstructural parameters on the mechanical properties of oxide dispersion strengthened Fe-14Cr steels, Acta Mater. 127 (2017) 165–177.
[46] P. Song, J. Gao, K. Yabuuchi, A. Kimura, Ion-irradiation hardening accompanied by irradiation-induced dissolution of oxides in FeCr(Y, Ti)-ODS ferritic steel, J. Nucl. Mater. 511 (2018) 200–211.